JART VCM v1 Verilog-A Compact Model

User Guide

Christopher Bengel, David Kaihua Zhang, Rainer Waser,
Stephan Menzel

Electronic Materials Research Laboratory

RWTH Aachen University
Forschungszentrum Jülich

May 2021

Table of Contents

Chapter 1

Scope of the Model

The Jülich Aachen Resistive Switching Tool (JART) VCM v1 is a set of SPICE-level, physics-based compact models describing bipolar resistive switching devices based on the valence change mechanism (VCM)-type Redox-based Resistive Random Access Memory (ReRAM).

The JART VCM v1 model is available in the following versions

1. JART VCM v1a [1][2][3]
2. JART VCM v1b
   (a) Deterministic [4]
   (b) Variability [5]
   (c) Random Telegraph Noise (RTN) [6]

The JART VCM v1a model was developed to simulate the switching characteristics of ReRAM devices based on the valence change mechanism. In this model, the ionic defect concentration (oxygen vacancies) in the disc region close to the active electrode (AE) defines the resistance state (see Fig.2.1). The concentration changes due to the drift of the ionic defects. Furthermore, these oxygen vacancies act as mobile donors and modulate the Schottky barrier at the AE/oxide interface. In this model, Joule heating is considered, which significantly accelerates the switching process at high current levels.

Since the JART VCM v1b model represents an improvement of the JART VCM v1a model, this user guide will have its focus on the JART VCM v1b model. Here, the equivalent circuit diagram (ECD) as well as some equations have been modified to explain the switching dynamics more accurately [4].

Based on the JART VCM v1b model, a variability model was developed, which includes both device-to-device and cycle-to-cycle variability. In terms of the device-to-device variability, the VCM cells are initiated with statistical distributed parameters: filament lengths, filament radii and maximum and minimum values for the oxygen vacancy concentration in the disc. The cycle-to-cycle variability is achieved by changing the four quantities during SET and RESET [5].

The latest extension of the JART VCM v1b also includes RTN, which is based on statistical jumps of oxygen vacancies into and out of the disc region [6].

The fundamentals of the VCM cell will firstly be discussed in Chapter 2. Following that, the compact model is introduced in Chapter 3, where the physical underlying equations are explained in more detail. To give the reader more intuitiveness for the model behavior, each parameter will be analyzed for its influence on the *I*-*V*-characteristics. Finally, some model *I*-*V* curves and as well as pulse characteristics of the model will be shown. In chapter 4, the variability module will be covered in more detail. In the last chapter 5, the RTN extension will be explained.

All simulations were performed using Cadence Spectre Circuit Simulator (Version 2018-2019). All our models are available at: http://www.emrl.de/JART.html.

Chapter 2

Valence Change Memory (VCM)

A Valence Change Mechanism (VCM) based memory cell consists of a metal-insulator-metal (MIM) system, where the insulator is typically a transition metal oxide (MO). The electrode materials are different with regards to their oxygen affinity and work function, which results in an asymmetrical material stack: at the interface between the electrically active electrode (AE), which exhibits a high work function and a low oxygen affinity, a Schottky barrier is formed. For the counter electrode, a metal with a low work function and high oxygen affinity is chosen. This electrode is referred to as the ohmic electrode (OE), as it forms an ohmic contact with the metal oxide.

The switching mechanisms in a VCM device between a high resistive state (HRS) and low resistive state (LRS) is illustrated in Fig. 2.1. During an initial forming step, the metal oxide is reduced, leaving behind a highly n-conductive filament with a high concentration of oxygen vacancies, which act as mobile donors. Two regions can be generally distinguished (see the inset in Fig. 2.1), the disc region and the plug region. The switching takes place in the disc region, a spatially confined region near the interface between the AE and the MO. Here, the local redox processes during switching, which can be expressed as an ionic motion of the oxygen vacancies, lead to a modulation of the Schottky barrier, which in turn alters the conductivity of the VCM cell. The plug region contains the main oxygen deficient filament and remains highly n-conductive during the whole switching process. Given the voltage is applied to the active electrode while the ohmic electrode is grounded, one obtains a typical *I*-*V*-characteristic as presented in Fig. 2.1. In the HRS, which is depicted in Fig. 2.1Ⓐ, the disc region is fully oxidized, resulting in a low conductivity in the VCM device. A negative voltage applied to the AE leads to the SET process (see Fig. 2.1Ⓑ), where the positively charged oxygen vacancies (indicated with green spheres) in the plug are attracted into the disc. A valence change of the metal ions (purple spheres) occurs, while the width and height of the

Schottky barrier is also decreased. After the SET, the device is in the LRS (Fig. 2.1Ⓒ). The RESET occurs for positive voltages applied to the AE. Here, the oxygen vacancies are pushed back into the plug region (Fig. 2.1Ⓓ), restoring the Schottky barrier to its former width and height. The shown *I-V* characteristics along with its switching is classified as bipolar switching, as the RESET and SET occur at different voltage polarities. Added to that, the switching mechanism based on the redistribution of oxygen vacancies in the filament is often called counter-eightwise (c8w) switching, which refers to the drawing direction of the *I-V* curve that resembles that of a oppositely handwritten, tilted ”8” [7].

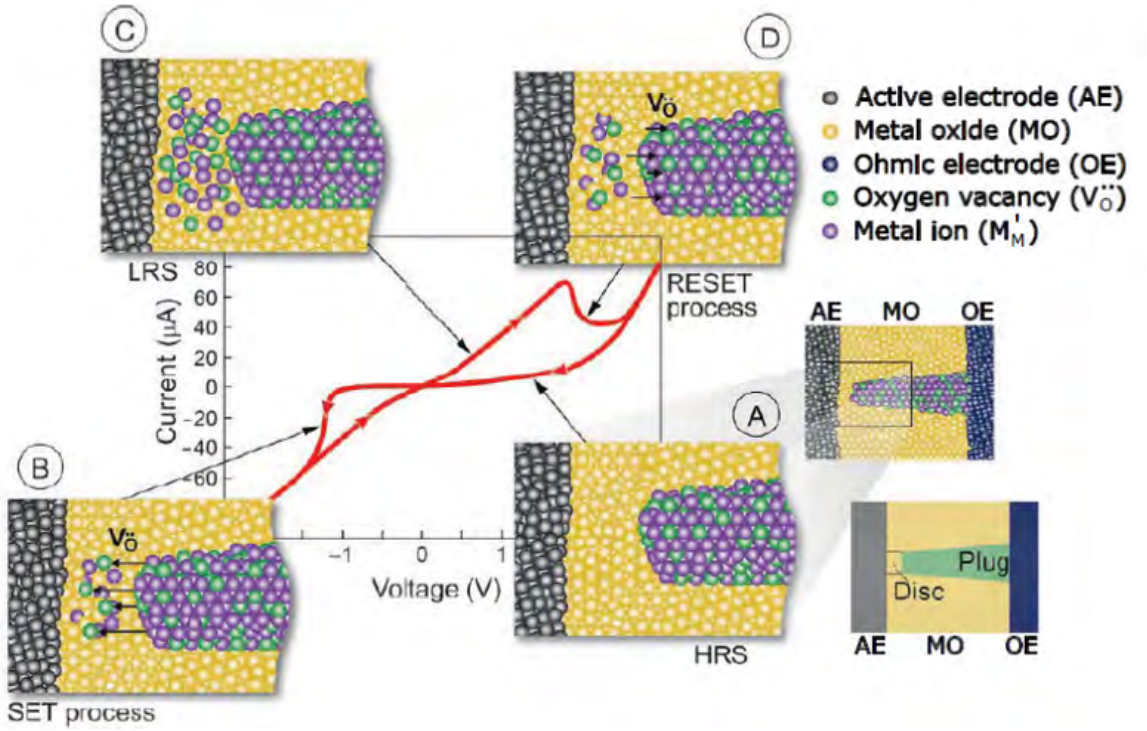

Fig. 2.1: Switching mechanism in a bipolar switching VCM cell. (a) Schematic *I-V*-curve with illustrations of the different switching stages. The green and purple spheres indicate the mobile oxygen vacancies and the immobile metal ions in a lower valence state, respectively. (A) high resistive state (HRS); (B) SET process; (C) low resistive state (LRS) and (D) RESET process. Modified and taken from [8]. Original from [7].

Chapter 3

JART VCM v1 Model

3.1 JART VCM v1b Deterministic

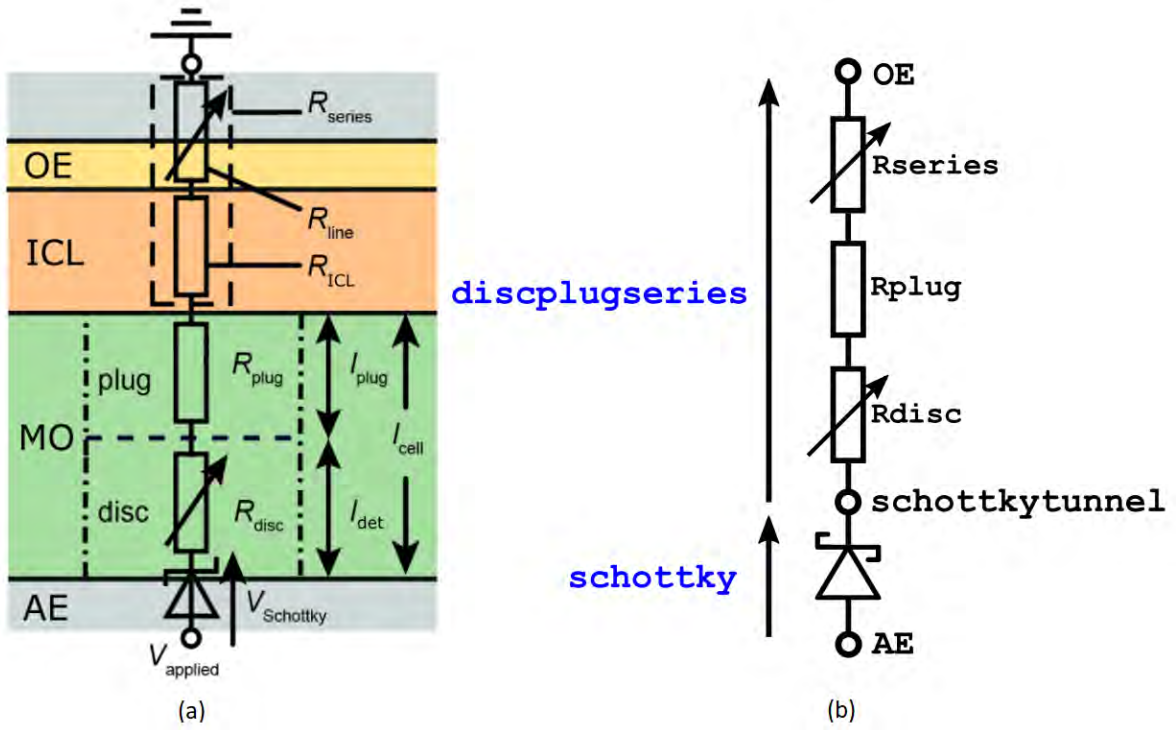

Fig. 3.1: Equivalent circuit diagram of the JART VCM v1b model (a) along with the electrical model in Verilog-A (b).

An equivalent circuit diagram of the electrical model is shown in Fig. 3.1 (a). The VCM cell considered in the JART VCM v1b model utilizes an additional inherent conduction layer (ICL), which reportedly has a positive impact on reducing the SET and HRS variability [1].

Fig. 3.1 (b) shows the electrical model in Verilog-A. Three electrical nodes are defined: AE, schottkytunnel and OE. The branch schottky connects the nodes AE and schottkytunnel, while the branch discplugseries connects the nodes schottkytunnel and OE.

In this manual, the voltage is applied to the AE while the OE is grounded. Consequently, the SET takes place in the negative voltage regime and the RESET occurs in the positive voltage regime. In the following, the underlying physical equations along with the Verilog-A code snippets are discussed in more detail.

Temperature and Joule Heating

For the whole filament, a homogeneous temperature T is assumed. The power dissipation over the cell P_{cell}, which consists of the Schottky contact, the disc region and the plug region, leads to a Joule heating in the device. This can be described as

$$T = P_{\text{cell}} R_{\text{th}} + T_0 = I \cdot (V_{\text{disc}} + V_{\text{plug}} + V_{\text{schottky}}) \cdot R_{\text{th, SET/RESET}} + T_0. \tag{3.1}$$

Here, V_{Schottky}, V_{disc} and V_{plug} are the voltage drops over the Schottky contact, the disc region and the plug region, respectively. $R_{\text{th, SET/RESET}}$ is the thermal resistance, which is chosen differently for the negative (SET) and positive (RESET) voltage polarity in order to describe the switching dynamics more accurately. Particularly, $R_{\text{th, RESET}}$ is scaled with a factor $R_{\text{theff, scaling}}$: $R_{\text{th, RESET}} = R_{\text{th, eff, scaling}} \cdot R_{\text{th0}}$, while $R_{\text{th, SET}} = R_{\text{th0}}$. The scaling of $R_{\text{th, RESET}}$ was motivated by continuum model simulation of the thermal properties of a Schottky contact and allows achieving a consistent description of the SET and RESET dynamics. T_0 denotes the ambient temperature.

In Verilog-A, the thermal description is realized by using the thermal discipline.

```
//Thermal branch for temperature calculation
thermal t;
branch (t) rth_branch;
branch (t) ith_branch;

...
 Pwr(ith_branch) <+ -(V(schottky)+V(discplugserial)*(Rdisc+Rplug)
                   /(Rdisc+Rplug+Rseries))*I(schottky);
 Pwr(rth_branch) <+ Temp(rth_branch)/Rtheff;
 Pwr(rth_branch) <+ ddt(Temp(rth_branch));
 Treal = T0 + Temp(rth_branch); // Equation (3.1)
```

Schottky contact at the AE/MO interface

The AE/MO junction is modeled as a Schottky diode. The nominal Schottky barrier height ϕ_{Bn0}, which is given by the difference between the work function of the AE and the electron affinity of the MO, is lowered by the Schottky effect. This results in an effective Schottky barrier height ϕ_{Bn}:

$$\phi_{Bn} = \phi_{Bn0} - e\sqrt[4]{\frac{e^3 z_{V_O} N_{disc}(\phi_{Bn0} - \phi_n - V_{schottky})}{8\pi^2 \varepsilon_{\phi_B}^3}}. \tag{3.2}$$

z_{V_O} is the charge number of an oxygen vacancy and N_{disc} is the oxygen vacancy concentration in the disc. ϕ_n denotes the energy difference between the unchanged conduction band and the Fermi level in the metal oxide and ε_{ϕ_B} is the permittivity related to the Schottky effect.

```
if (V(schottky)<phiBn0-phin)
   begin
      psi=phiBn0-phin-V(schottky);
      phiBn=phiBn0-sqrt(sqrt(pow('P_Q,3)*zvo*Nreal*1e26*psi/
            (8*pow('M_PI,2)*(pow(epsphib_eff,3))))); // Equation (3.2)
      if (phiBn<0)
         begin
            phiBn=0;
         end
   end
else
   begin
      psi=0;
      phiBn=phiBn0;
   end
```

In the listing it can be seen that the oxygen vacancy concentration in the disc is scaled by 1e26. This is done to improve the convergence behavior of the model. The current conduction across the Schottky barrier can be divided into the forward and reverse direction: in forward direction ($V_{applied} > 0$ V), the dominant current conduction mechanism is assumed to be the thermionic emission (TE), where electrons overcome the Schottky barrier by thermal excitation. Thermionic emission is calculated according to [9] as

$$I_{V_{applied}>0\,V} = I_{schottky,\,TE} = AA^*T^2 \exp\left(\frac{-e\phi_{Bn}}{k_B T}\right)\left[\exp\left(\frac{eV_{Schottky}}{k_B T}\right) - 1\right]. \tag{3.3}$$

A is the cross sectional area of the filament, $A = \pi r_{\mathrm{det}}^2$, with r_{det} as the radius of the filament, A^* is the Richardson constant, e is the elementary charge and k_{B} is the Boltzmann constant.

In reverse direction ($V_{\mathrm{applied}} < 0$ V), the thermionic field emission (TFE), which involves a thermally-assisted tunneling through the Schottky barrier, is assumed to be the dominant electronic conduction mechanism. The current can be expressed with

$$I_{\mathrm{V_{applied}<0\,V}} = I_{\mathrm{schottky,\,TFE}} = -A\frac{A^*T}{k_{\mathrm{B}}}\sqrt{\pi W_{00} e\left(-V_{\mathrm{Schottky}} + \frac{\phi_{\mathrm{Bn}}}{\cosh^2(\frac{W_{00}}{k_{\mathrm{B}}T})}\right)} \cdot \exp\left(\frac{-e\phi_{\mathrm{Bn}}}{W_0}\right)\left(\exp\left(\frac{-eV_{\mathrm{Schottky}}}{\varepsilon'}\right) - 1\right). \tag{3.4}$$

with W_{00} as

$$W_{00} = \frac{eh}{4\pi}\sqrt{\frac{z_{\mathrm{Vo}} N_{\mathrm{disc}}}{m^* \varepsilon_{\mathrm{s}} e}}, \tag{3.5}$$

where m^* is the effective mass of the electron and ε_{s} is the static permittivity. W_0 can then be described as

$$W_0 = W_{00}\coth\left(\frac{W_{00}}{k_{\mathrm{B}}T}\right), \tag{3.6}$$

and ε' as

$$\varepsilon' = \frac{W_{00}}{\frac{W_{00}}{k_{\mathrm{B}}T} - \tanh(\frac{W_{00}}{k_{\mathrm{B}}T})}. \tag{3.7}$$

```
if (V(schottky)<0) //TFE Reverse Direction
   begin
      W00=('P_Q*h/(4*'M_PI))*sqrt(zvo*Nreal*1e26/(mdiel*eps_eff));  // Equation (3.5)

      W0=W00/tanh(W00/('P_K*Treal));                               // Equation (3.6)

      epsprime=W00/(W00/('P_K*Treal)-tanh(W00/('P_K*Treal)));  // Equation (3.7)

      Ischottkytunnel=-A*Arichardson*Treal/'P_K*sqrt('M_PI*W00*'P_Q*
      (abs(V(schottky))+phiBn/pow(cosh(W00/('P_K*Treal)),2)))*
      exp(-'P_Q*phiBn/W0)*(exp('P_Q*abs(V(schottky))/epsprime)-1); // Equation (3.4)
   end
else    //TE Forward Direction
   begin
      Ischottkytunnel= A*Arichardson*pow(Treal,2)*exp(-phiBn*'P_Q/('P_K*Treal))*
      (exp('P_Q/('P_K*Treal)*V(schottky))-1); // Equation (3.3)
   end
```

```
    I(schottky)<+Ischottkytunnel;
```

Disc resistance R_{disc}, plug resistance R_{plug}, Series resistance R_{series}

The disc and plug region of the filament in the MO-layer with a length of l_{cell} are modeled as resistances with

$$R_{\text{disc}} = \frac{l_{\text{det}}}{e z_{\text{Vo}} N_{\text{disc}} \mu_{\text{n}} A} \tag{3.8}$$

and

$$R_{\text{plug}} = \frac{l_{\text{plug}}}{e z_{\text{Vo}} N_{\text{plug}} \mu_{\text{n}} A}. \tag{3.9}$$

l_{det} and l_{plug} are the lengths of the disc and plug region, respectively. N_{plug} is the oxygen vacancy concentration in the plug and μ_{n} is the electron mobility. N_{plug} is kept constant and serves as an infinite reservoir of oxygen vacancies, while N_{disc} is the state variable in this system.

The series resistance R_{series} considers the constant resistance of the ICL R_{ICL} aswell as a current-dependent resistance of the lines contacting the device, R_{line}:

$$R_{\text{series}} = R_{\text{ICL}} + R_{\text{line}} = R_{\text{ICL}} + R_0 \cdot (1 + \alpha_{\text{line}} R_0 I^2 R_{\text{th,line}}), \tag{3.10}$$

Here, R_0 represents the line resistance at zero current, α_{line} represents the temperature coefficient of the line and $R_{\text{th, line}}$ is the thermal resistance of the line.

```
//Disc Resistance
Rdisc=1/(Nreal*1e26*zvo*'P_Q*un)*ldet*1e-9/A;                    // Equation (3.8)

//Plug Resistance
Rplug=(1/(Nplug*1e26*zvo*'P_Q*un)*(lcell-ldet)*1e-9/A);          // Equation (3.9)

//Series Resistance
Rline=R0*(1+R0*alphaline*pow(I(discplugseries),2)*Rthline);
Rseries=RseriesICL+Rline;                                      // Equation (3.10)
```

Change of the state variable N_{disc}

The time evolution of N_{disc} can be expressed with

$$\frac{dN_{\text{disc}}}{dt} = \frac{1}{z_{\text{V}_\text{O}} e A l_{\text{det}}} I_{\text{ion}}. \tag{3.11}$$

Here, I_{ion} denotes the ionic current into and from the disc region and is based on a field accelerated ionic hopping mechanism. According to Genreith-Schriever and De Souza [10], this ionic current can be calculated as

$$I_{\text{ion}} = z_{\text{V}_\text{O}} e A c_{\text{V}_\text{O}} a \nu_0 F_{\text{limit}} \cdot \left(\exp(-\frac{\Delta W_{\text{A,min}}}{k_\text{B} T}) - \exp(-\frac{\Delta W_{\text{A,max}}}{k_\text{B} T}) \right) \tag{3.12}$$

with c_{V_O} as the average concentration of the plug and disc.

$$c_{\text{V}_\text{O}} = \frac{N_{\text{plug}} + N_{\text{disc}}}{2}, \tag{3.13}$$

a is the ion hopping distance and ν_0 is the attempt frequency. F_{limit} serves as a limiting factor for the ionic current to keep the vacancy concentration in the disc N_{disc} between $N_{\text{disc, min}}$ and $N_{\text{disc, max}}$:

$$F_{\text{limit}} = \begin{cases} 1 - \left(\frac{N_{\text{disc,min}}}{N_{\text{disc}}} \right)^{10}, & \text{for } V_{\text{applied}} > 0 \text{ V} \\ \\ 1 - \left(\frac{N_{\text{disc}}}{N_{\text{disc,max}}} \right)^{10}, & \text{for } V_{\text{applied}} < 0 \text{ V}. \end{cases} \tag{3.14}$$

The exponent of 10 is chosen such that the ionic current is only influenced by F_{limit} when N_{disc} is close to its limits. $\Delta W_{\text{A,min}}$ and $\Delta W_{\text{A,max}}$ represent the activation energy for an ion jump in the direction of the electric field and in the opposite direction of the electric field, respectively. They can be expressed with

$$\Delta W_{\text{A,min}} = \Delta W_\text{A} \cdot (\sqrt{1-\gamma^2} - \gamma\frac{\pi}{2} + \gamma \arcsin \gamma) \tag{3.15}$$

and

$$\Delta W_{\text{A,max}} = \Delta W_\text{A} \cdot (\sqrt{1-\gamma^2} + \gamma\frac{\pi}{2} + \gamma \arcsin \gamma) \tag{3.16}$$

with γ as

$$\gamma = \frac{e z_{\text{V}_\text{O}} a E_{\text{SET/RESET}}}{\Delta W_\text{A} \pi}. \tag{3.17}$$

and ΔW_A as the nominal activation energy. E_{SET} is the electric field during the SET and given by

$$E_{SET} = \frac{V_{disc}}{l_{det}} \tag{3.18}$$

and E_{RESET} represents the electric field during the RESET with

$$E_{RESET} = \frac{V_{schottky} + V_{disc} + V_{plug}}{l_{cell}} = \frac{V_{cell}}{l_{cell}}. \tag{3.19}$$

In Verilog-A, the ionic current is defined as a voltage source. This is done since the integration operator "idt" can only be applied to signals which will have a nature and no concentration nature is available. In case $N_{disc,max}$ or $N_{disc,min}$ is reached, the ionic current is set to zero.

```
///calculation of the concentration
Nchange=idt(-1/(A*ldet*1e-9*'P_Q*zvo)*V(ion,gnd)/1e26,0); // Equation (3.11)
Nreal=Ninit + Nchange;
V(N,gnd)<+Nreal;

if (((Nreal<Ndiscmin)&(V(AE,OE)>0))|((Nreal>Ndiscmax)&(V(AE,OE)<0))) // keep
    concentration Nreal in the borders of Ndiscmin and Ndiscmax
   begin
      V(ion,gnd)<+0;
   end
else
   begin
      cvo = (Nplug+Nreal)/2*1e26; // Equation (3.13)
      if (V(AE,OE)>0) //RESET
         begin
            E_ion=(V(schottky)+V(discplugseries)*(Rdisc+Rplug))/
                  (Rdisc+Rplug+Rseries)/(lcell*1e-9); // Equation (3.19)
            Rtheff = Rth0*Rtheff_scaling;
            Flim=1-pow(Ndiscmin/Nreal,10); // Equation (3.14)
         end
      else
         begin
            E_ion=V(discplugseries)*Rdisc/(Rdisc+Rplug+Rseries)
                  /(ldet*1e-9); // Equation (3.18)
            Rtheff = Rth0;
            Flim=1-pow(Nreal/Ndiscmax,10); // Equation (3.14)
         end
```

```
    gamma=zvo*'P_Q*E_ion*a/('M_PI*dWa*'P_Q); // Equation (3.17)
    dWamin=dWa*'P_Q*(sqrt(1-pow(gamma,2))-gamma*'M_PI/2+gamma*asin(gamma)); // Eq.
        (3.15)
    dWamax=dWa*'P_Q*(sqrt(1-pow(gamma,2))+gamma*'M_PI/2+gamma*asin(gamma)); // Eq.
        (3.16)

    V(ion,gnd)<+zvo*'P_Q*cvo*a*ny0*A*(exp(-dWamin/('P_K*Treal))-
              exp(-dWamax/('P_K*Treal)))*Flim; // Equation (3.12)
  end
  end
```

To further ensure, that the concentration are kept within the specified boundaries, the step size is dynamically adjusted during an abrupt SET or RESET.

```
   V(slopeN,gnd)<+ddt(V(N,gnd))/V(N,gnd)*1e-12;
if ((abs(V(slopeN,gnd))>1e-3))
  begin
    $bound_step(1e-11);
  end
```

3.1.1 Constants and Parameters

Table 3.1 summarizes all constants used in the Verilog-A model.

Constant name	Symbol	Description	Value	Unit
‘M_PI	π	Pi	3.1415927	
‘P_Q	e	Charge of an electron	$1.6022 \cdot 10^{-19}$	C
‘P_K	k_B	Boltzmann’s constant	$1.38065 \cdot 10^{-23}$	J/K
‘P_EPS0	ε_0	Permittivity of a vacuum	$8.65419 \cdot 10^{-12}$	F/m
Arichardson	A^*	Effective Richardson constant	$6.01 \cdot 10^{5}$	A/m^2K^2
mdiel	m^*	Electron rest mass	$9.10938 \cdot 10^{-31}$	kg
zvo	z_{V_O}	Oxygen vacancy charge number	2	

Table 3.1: List of constants. Those denoted with an ’ belong to constants.vams.

In Table 3.2, all device parameters including their suggested ranges are shown. Note that not all possible parameter combinations have been tested and convergence issues might arise for certain parameter sets.

Parameter name	Symbol	Description	Range	Unit
T0	T_0	Ambient temperature	[100 ; 500]	K
eps	ε_s	Static Permittivity	[10 ; 25]	-
epsphib	$\varepsilon_{\phi_{Bn0}}$	Permittivity related to the Schottky effect	[1 ; 10]	-
phiBn0	ϕ_{Bn0}	Nominal Schotty barrier height	[0.1 ; 1.5]	eV
phin	ϕ_n	Energy level difference between the Fermi level in the oxide and the oxide conduction band edge	[0.1 ; ϕ_{Bn0}]	eV
un	μ_n	Electron Mobility	[1e-6 ; 1e-5]	$m^2/(Vs)$
Ndiscmax	$N_{disc,max}$	Maximum oxygen vacancy concentration in the disc	[0.001 ; 1100]	$10^{26}/m^3$
Ndiscmin	$N_{disc,min}$	Minimum oxygen vacancy concentration in the disc	[0.0001 ; 100]	$10^{26}/m^3$
Ninit	N_{init}	Initial oxygen vacancy concentration in the disc	[0.0001 ; 1000]	$10^{26}/m^3$
Nplug	N_{plug}	Inital oxygen vacancy concentration in the plug	[0.001 ; 100]	$10^{26}/m^3$
a	a	Ion hopping distance	[1e-10 ; 1e-9]	m
ny0	ν_0	Attempt frequency	[1e10 ; 1e14]	Hz
dWa	ΔW_A	Activation energy for ion hopping	[0.8 ; 1.5]	eV
Rth0	R_{th0}	Thermal resistance	[1e6 ; 2e7]	W/K
rdet	r_{det}	Radius of the filament	[5e-9 ; 100e-9]	m
lcell	l_{cell}	Length of the filament	[2 ; 5]	nm
ldet	l_{det}	Length of the disc	[0.1 ; l_{cell}]	nm
Rtheffscaling	$R_{theff,scaling}$	Scaling factor of the thermal resistance for gradual RESET	[0.1 ; 1]	-
RseriesICL	$R_{series,ICL}$	Series resistance of the ICL layer	[100 ; 2e5]	Ω
R0	R_0	Line resistance for a current of 0 A		Ω
Rthline	$R_{th,line}$	Thermal resistance of the lines		W/K
alphaline	α_{line}	Temperature coefficient in the lines		1/K

Table 3.2: List of device parameter with suggested ranges.

3.1.2 Model Instantiation for Transient Simulation

In the following, we will explain how to to include the model into a Spectre netlist. It is also possible to copy the code into a Verilog-A Cellview and to create a symbol for the Schematic Editor. Before instantiating the model, the Verilog-A code has to be included into the netlist.

```
ahdl_include "JART-VCM-v1.va"
```

If the model is not saved in the current directory, the complete path to the model has to be specified in the include command. The model can now be instantiated with the following code. The provided parameter set has been fitted to describe the switching dynamics in HfO_x based VCM cells [4].

```
I8 (AE 0) JART_VCM_1b_det T0=0.293 eps=17 epsphib=5.5 phiBn0=0.18 \
       phin=0.1 un=4e-06 Ndiscmax=20 Ndiscmin=0.008 Ninit=0.008 Nplug=20 \
       a=2.5e-10 ny0=2e+13 dWa=1.35 Rth0=10e6 rdet=45e-9 lcell=3 \
       ldet=0.4 Rtheff_scaling=0.27 RseriesTiOx=650 R0=719.244 \
       Rthline=90471.5 alphaline=0.00392
```

The code below shows an example on how to setup the simulation environment including the numerical settings. The following code simulates a triangular voltage sweep between -2 V and 2 V which is applied to the active electrode over a time period of 8 s. To ensure a reasonably well time resolution of the transients, one should consider a maximal timestep of `maxstep` = 0.001 s or less.

```
V3 (AE 0) vsource type=pwl wave=[ 0 0 1.5 -1.5 3 0 4.5 1.5 6 0 ]
simulatorOptions options vabstol=1e-6 \
iabstol=1e-12 temp=27 tnom=27 gmin=1e-12 \
tran tran stop=8 errpreset=conservative maxstep=1e-3
```

In order to plot the transients of the oxygen vacancy concentration or the temperature, all signals can be saved by using

```
saveOptions options save=all currents=all saveahdlvars=all
```

3.2 Model Characteristics

The model characteristics are shown in Fig. 3.2, which were obtained by using the parameter set and simulation environment provided in the Listings in Chapter 3.1.2. In the *I*-*V*-characteristics

in Fig. 3.2a, the switching directions are marked with the solid arrows. The dotted arrows mark the SET voltage V_{SET} and the RESET voltage V_{RESET}. Fig. 3.2b). During the SET process, the oxygen vacancy concentration in the disc N_{disc} increases abruptly (see Fig. 3.2b) up to $N_{\mathrm{disc,\,max}}$. The abruptness of the SET originates from a thermal feedback, which can be seen at the spike in Fig. 3.2c. For $V_{\mathrm{applied}} > 0$ V, the RESET occurs, during which the oxygen vacancy concentration decreases to $N_{\mathrm{disc,min}}$. The abrupt decrease in conductivity is followed by a more gradual decrease, which stems from the negative feedback between the temperature, the ionic movement and the current.

The interplay of the resistances in the device is illustrated in Fig. 3.2d. It is evident, that the disc resistance dominates the HRS, whereas in the LRS, the series resistance consisting of the line resistance and ICL resistance limits the current.

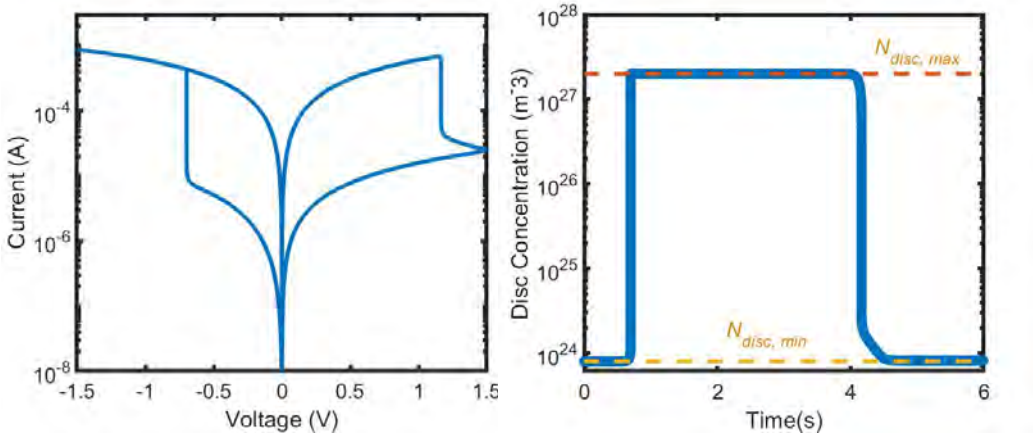

(a) *I-V*-characteristic **(b)** Oxygen vacancy concentration in the disc

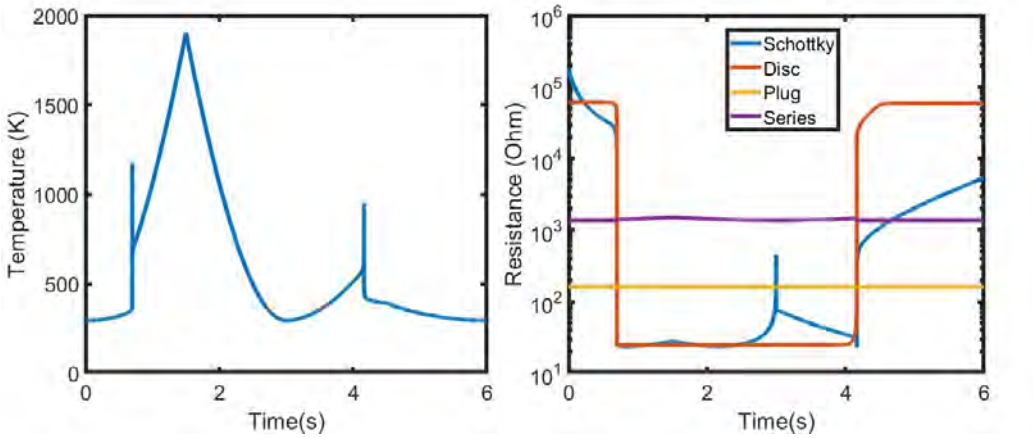

(c) Temperature over time **(d)** Resistance components over time

Fig. 3.2: Model Characteristics obtained by applying a triangular *I-V*-sweep between -1.5 V and 1.5 V.

3.2.1 Influence of the Model Parameters

In order to give the reader a better understanding and intuitivity of the underlying model parameter, each parameter will be discussed with regard to their physical influence on the LRS, the HRS and the absolute SET and the RESET voltages. The following explanations are based on the simulations obtained by using the basic parameters in the Listing 3.1.2. Note, that the behavior of the model might slightly vary depending on how the parameter set is chosen. The general trends however should hold.

Ambient Temperature (T_0)

The switching kinetics are mainly a temperature driven processes [11]. When the ambient temperature is increased, more thermally excited electrons are generated. This leads to a higher current across the Schottky contact, which is the limiting component in the HRS for $V_{\text{applied}} < 0$ V. Furthermore, less additional Joule heating (power generated) is needed to achieve sufficient thermal energy for the activation of the ionic movement. The SET and RESET consequently will occur at lower absolute voltages.

Static Permittivity (ε_{s}) and Permittivity Related to the Schottky Effect ($\varepsilon_{\phi_{\text{Bn0}}}$)

Both ε_{s} and $\varepsilon_{\phi_{\text{Bn0}}}$ are related to the conduction mechanism at the Schottky barrier. While ε_{s} only influences the thermionic field emission ($V_{\text{applied}}< 0$ V), $\varepsilon_{\phi_{\text{Bn0}}}$ is connected to the Schottky effect and hence has an effect on both TE and TFE. Generally, both describe the screening of a charged region by the polarization of the material. The increase of ε_{s} and $\varepsilon_{\phi_{\text{Bn0}}}$ increases the HRS for $V_{\text{applied}} < 0$ V, in which a noticeable voltage drop over the Schottky diode can be seen. Also the SET voltage is increased. Increasing $\varepsilon_{\phi_{\text{Bn0}}}$ also increases the HRS for $V_{\text{applied}} > 0$ V

Nominal Schottky Barrier (ϕ_{Bn0})

The nominal Schottky barrier is the main parameter to choose for controlling the influence of the Schottky diode in the device. In the suggested range, ϕ_{Bn0} will mainly have an impact on the HRS regime for $V_{\text{applied}} < 0$ and for larger values also on the HRS regime for $V_{\text{applied}} > 0$. As one can see in Fig. 3.3c, the increase of the nominal Schottky barrier leads to a higher HRS, and by that to a shift of the SET V_{SET} towards higher absolute voltages.

Energy Level Difference (ϕ_n)

This quantity only appears in the field dependent barrier lowering term in Eq. 3.1. Under zero bias, the nominal Schottky-barrier is already lowered by the non-zero electric field present at the AE/MO-interface, which originates from the built-in potential given by difference of ϕ_{Bn0} and ϕ_n. As a result, when ϕ_n is increased, the Schottky effect caused by the built-in potential will decrease. Note that ϕ_n must not exceed ϕ_{Bn0}! For the provided parameter set, the effect of ϕ_n is mainly present in the HRS for $V_{applied}< 0$ V, as only there is a significant voltage drop across the Schottky-diode.

Electron Mobility (μ_n)

The electron mobility μ_n is inversely related to the the disc and plug resistance. An increase of μ_n will lead to a higher conductivity in the filament. On the one side, this results in a lower HRS and hence a smaller absolute SET voltage, but on the other side it also leads to a lower LRS and to a shift of the RESET towards higher voltages. The latter shift is due to the higher conductivity of the disc and plug region and the accompanying lesser voltage drop across these regions, which in turn decreases the electric fields that accelerates the ionic movement for $V_{applied}> 0$ V. On top of that, the RESET becomes more abrupt. This can be explained by a shift of the voltage divider relationship between series and device resistance towards the series resistance [1].

Minimum Oxygen Vacancy Concentration in the Disc ($N_{disc,\,min}$)

The influence of $N_{disc,\,min}$ on the I-V-characteristics is shown in Fig. 3.3a. $N_{disc,\,min}$ limits the maximum amount of oxygen vacancies migrated out of the disc during the RESET.

Initial Oxygen Vacancy Concentration in the Disc (N_{init})

The influence of N_{init} on the I-V-characteristics is shown in Fig. 3.3a. It is recommended to keep the initial oxygen vacancy concentrations the same as either $N_{disc,\,min}$ or $N_{disc,\,max}$), so that a better control of the resistance states is given. It is apparent, that N_{init} (N_{min}) can be used to adjust the HRS without changing the LRS. The absolute SET voltage also gets shifted towards smaller voltages with increasing N_{init}.

Maximum Oxygen Vacancy Concentration in the Disc ($N_{\text{disc, max}}$)

The influence of $N_{\text{disc, max}}$ on the I-V-characteristics is shown in Fig. 3.3b. $N_{\text{disc, max}}$ limits the maximum amount of oxygen vacancies migrated into the disc during the SET. Up to a certain $N_{\text{disc, max}}$, the LRS is determined by the disc resistance. Once the $N_{\text{disc, max}}$ gets even larger, the disc becomes too conductive and the LRS is mainly determined by the series resistance R_{series}. Added to that, the RESET will get shifted towards higher voltages.

Initial Oxygen Vacancy Concentration in the Plug (N_{plug})

In this model, the oxygen vacancy concentration in the plug N_{plug} and by that the plug resistance R_{plug} does not change during the switching process. As the model assumes the plug region to serve as an infinite reservoir of oxygen vacancies. Commonly the oxygen concentration in the plug is set to the maximum value specified by $N_{\text{disc, max}}$.

Ion Hopping Distance (a) and Attempt Frequency (ν_0)

Both quantities appear as prefactors of the ionic current in Eq. 3.1, so their influence on the I-V-characteristics are similar. The increase of either a or ν_0 will lead to a larger ionic current, which in turn will lead to a SET and RESET at smaller absolute voltages. However, the HRS as well as the LRS are not affected by a change of these parameters, as no ionic current is present in these states due to the limiting factor F_{lim}.

Activation Energy for Ion Hopping (ΔW_{A})

Similar to the ion hopping distance a and the attempt frequency ν_0, the nominal activation energy for ion hopping ΔW_{A} determines the SET and RESET voltage, i.e. a higher activation energy will require more thermal energy to excite the ions, thus resulting in a SET and RESET at higher absolute voltages. The effective activation energy also varies for $V_{\text{applied}} < 0$ V and $V_{\text{applied}} > 0$ V due to an additional influence of the electric field (see Eq. 3.1 and Eq. 3.1). The HRS and LRS will not be affected by a change of ΔW_{A} (see Fig. 3.3d).

Thermal Resistance (R_{th0})

The thermal resistance acts as the conversion factor between the power dissipated in the cell and the temperature increase in the VCM device. An increase of the thermal resistance will thus lead to more heat generated by the same amount of dissipated power. This can be observed as an earlier SET and RESET in the I-V-characteristics. The LRS and the HRS however are

quite unaffected by the Joule heating: as for the HRS, the power dissipated over the device for the suggested range of R_{th0} is so small, that the temperature increase only has a marginal effect on the current. As for the LRS, the series resistance R_{series}, which is independent from the cell temperature, limits the current.

Radius of the Filament (r_{det})

The quantities, which depend on the radius of the filament r_{det}, are the current conduction mechanisms at the Schottky diode (Eq. 3.3 and Eq. 3.4), the disc resistance R_{disc} and the plug resistance R_{plug}. An increase of r_{det} will result in an increase in conductance of the mentioned Schottky diode, disc and plug region, hence leading to a smaller HRS. The SET voltage is shifted towards smaller absolute voltages while the RESET is shifted towards higher voltages due to a smaller voltage drop across the disc and plug region.

Length of the Filament (l_{cell})

When the length of the filament l_{cell} is increased in the given range, the LRS will get less conductive, as the plug resistance R_{plug} increases ($R_{plug} = R_{cell} - R_{disc}$). This effect however is only marginal, since the R_{Series} is still the dominant resistance in the LRS. One can also observe a shift of the RESET voltage towards higher voltages, since the electric field during the RESET E_{RESET} (see Eq. 3.1) is reduced. Note that the length of the filament has to be at least l_{disc} or larger.

Length of the Disc l_{det}

The increase of the length of the disc l_{det} will on the one hand increase the disc resistance R_{disc}, which is the dominant resistance in the HRS, and on the other hand, the electric field during the SET E_{SET} (see Eq. 3.1) is decreased, thus shifting the absolute SET voltage towards higher voltages (see Fig. 3.3e).

Scaling Factor of the Thermal Resistance For the Gradual RESET ($R_{theff,\,scaling}$)

The scaling factor determines the value of the thermal resistance for $V_{applied}$> 0 V, which is given by $R_{th,\,RESET} = R_{theff,\,scaling} \cdot R_{th0}$. The increase of $R_{theff,\,scaling}$ will result in a higher temperature increase per power dissipated. The RESET will then get shifted towards smaller voltages (see Fig. 3.3f).

Series Resistance of the Inherent Conduction Layer ($R_{\text{series, ICL}}$)

In the provided parameter set, the resistance of the ICL belongs to the series resistance, which is the dominant resistance in the LRS regime. Consequently, an increase of $R_{\text{series, ICL}}$ will result in a lower LRS and the RESET voltage will get shifted towards higher voltages, as less voltage drops across the plug and disc region.

Line Resistance for a current of 0 A (R_0)

The line increases in resistance by self-heating. R_0 has the same effect on the I-V-characteristics as the series resistance of the ICL, except its additional dependency on the Joule heating.

Thermal Resistance of the Lines ($R_{\text{th,line}}$) and Temperature Coefficient of the Lines (α_{line})

Both quantities scale the resistance increase of the line caused by the Joule heating over the line. Note that the increase of the line resistance does not depend on the temperature of the cell.

Increase of Parameter	$\lvert V_{SET} \rvert$ [V]	$\lvert V_{RESET} \rvert$ [V]	HRS [Ω]	LRS [Ω]
T0	-	-	0	0
eps	+	0	+	0
epshib	+	0	+	0
phiBn0	+	0	+	0
phin	+		+	
un	-	+	-	-
Ndiscmax	0	+	0	+(0)
Ninit (Ndiscmin)	-	0	-	0
Nplug	-	+	-	-
a	-	-	0	0
ny0	-	-	0	0
dWa	+	+	0	0
Rth0	-	-	0	0
rdet	-	+	-	0
lcell	0	-	0	0
ldet	+	0	+	0
Rtheffscaling	0	-	0	0
RseriesICL	0	+	-	+
R0	0	+	0	+
Rthline	0	+	0	+
alphaline	0	+	0	+

Table 3.3: Summary of the parameters and their influence on the *I-V* characteristics. + and - indicate the increase and decrease, respectively, while 0 indicate marginal to no change of the given quantity.

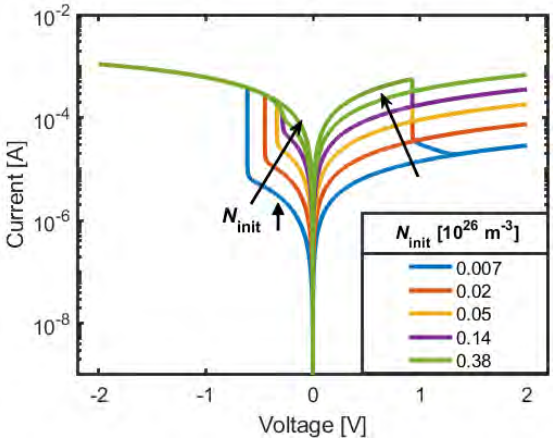

(a) Influence of `Ninit` and `Ndiscmin`

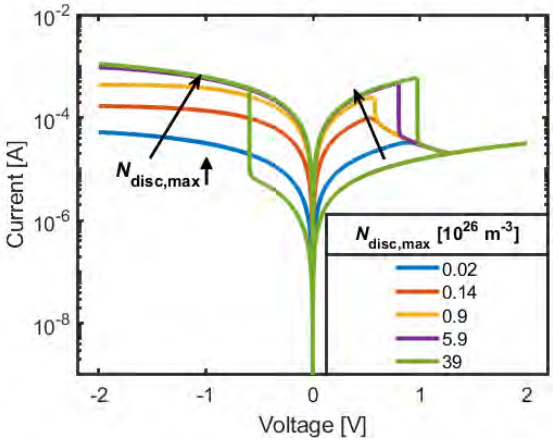

(b) Influence of `Ndiscmax`

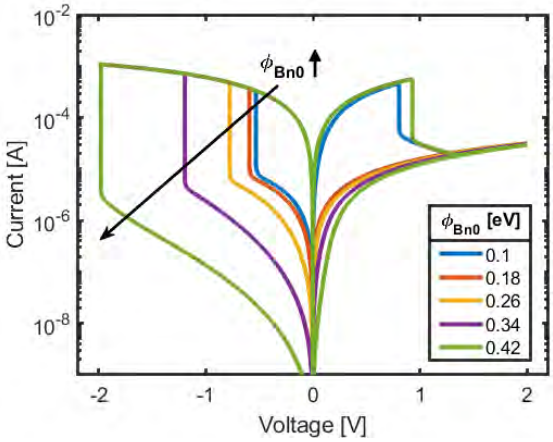

(c) Influence of `phiBn0`

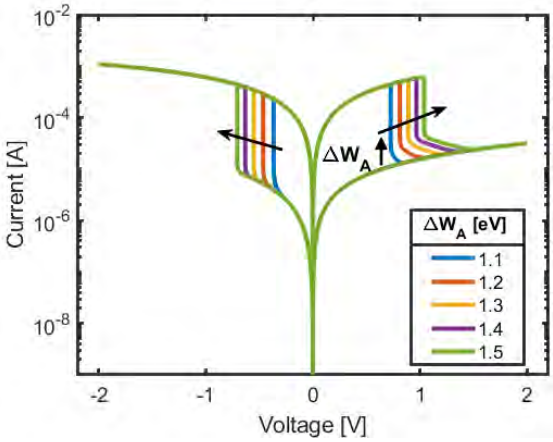

(d) Influence of `dWa`

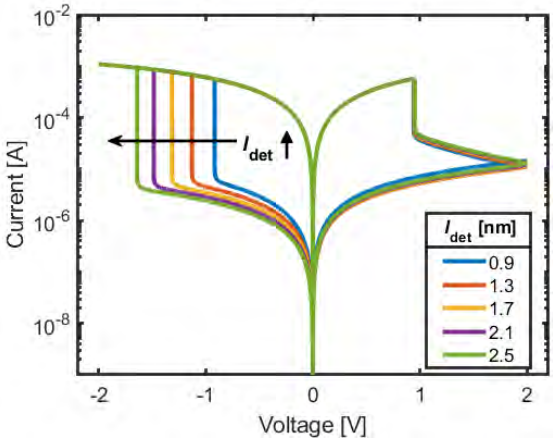

(e) Influence of `ldet`

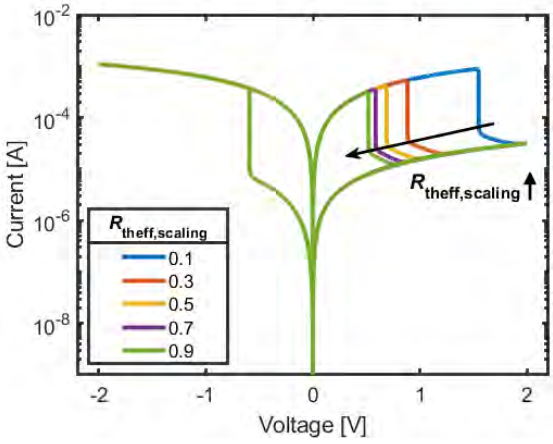

(f) Influence of `Rtheffscaling`

Fig. 3.3: Summary of some parameters with a large influence on the *I-V* characteristics.

3.3 Pulse Characteristics

The following section will show some examples of pulse simulations using the Verilog-A model. For further readings regarding pulse characteristics, please refer to [4]. In this chapter we exemplary showcase the dependence of the SET and RESET process on the initial resistive state of the device and the SET and RESET voltages.

3.3.1 SET

The pulse characteristic for a SET is shown in Fig. 3.4, with the blue curve depicting the applied voltage and the orange curve depicting the corresponding current. The READ voltage is set to 0.2 V, whereas the WRITE voltage is set to -0.75 V. The rise- and fall-time of the pulses are set to 1 ns, while the pulse width is 1 ms.

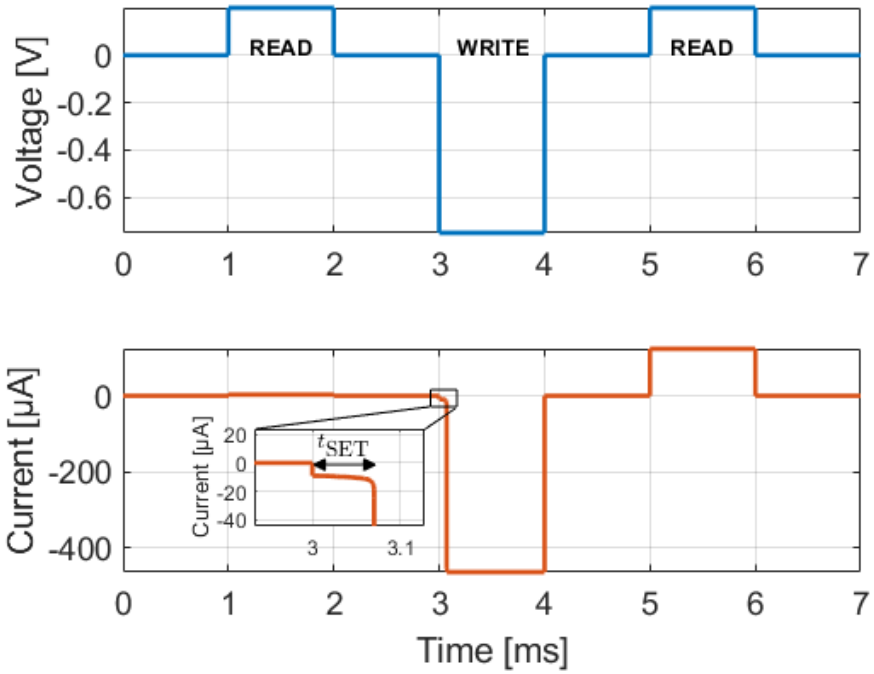

Fig. 3.4: Pulse Characteristics for SET: Read at 0.2 V and write at -0.75 V.

Notice that there is a small delay of t_{SET} between the start of the voltage pulse and the SET. This delay time depend on the initial HRS state of the device as well as on the SET pulse voltage and should be kept mind when simulating pulses on small time scales. The influence of delay time and initial state on the pulse characteristics is shown in Fig. 3.5. In Fig. 3.5a, the increase of the oxygen vacancy concentration in the disc lead to a smaller delay t_{SET}, which

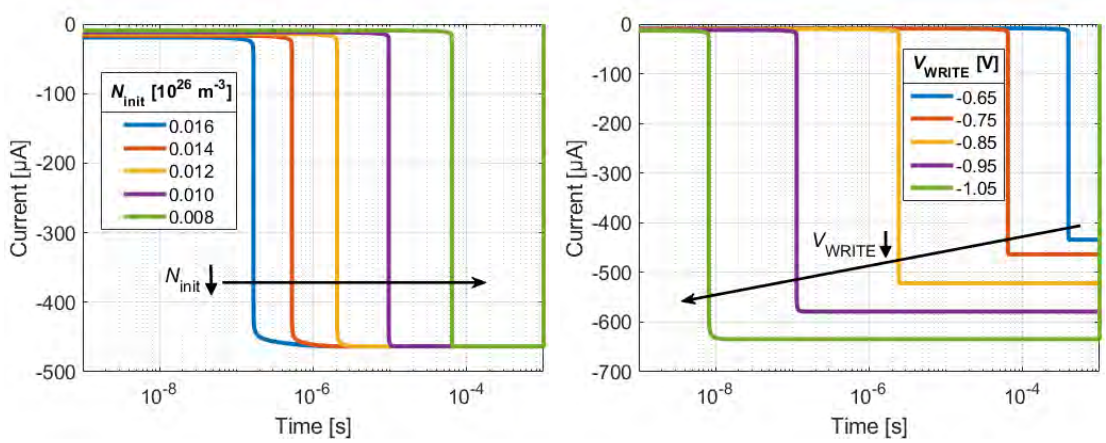

Fig. 3.5: State and voltage dependency of the SET delay time t_{SET} a) at different initial HRS ($V_{WRITE} = -0.75$ V and b) for different WRITE pulse voltages.

is due to the higher conductivity in the HRS and hence higher Joule heating. As for the SET pulse voltages, which is shown in Fig. 3.5b, a more negative voltage will lead to an earlier SET as the electric field is larger. It is also apparent, that the dependency of t_{SET} on both quantities is nonlinear. The behaviors shown here are in accordance with experimental studies [4, 12, 13].

3.3.2 RESET

The pulse characteristics involving the RESET of the VCM cell are shown in Fig. 3.6. Here, the READ voltage stays at 0.2 V, whereas the WRITE voltage is set to 1.5 V. The rise- and fall-time of the pulses are set to 1 ns and the pulse width is kept at 1 s. Similar to the SET pulse, the RESET is accompanied by a delay t_{RESET}, which again depend on the initial LRS and the RESET pulse voltage (see Fig. 3.7). In the LRS, almost the entire voltage drops across the series resistance R_{series}. By decreasing the initial disc concentration N_{init}, the voltage drop across the disc starts to increase. Consequently, the threshold electric field for the RESET is reached earlier. Furthermore, a higher temperature in the cell will be reached for smaller N_{init}, which further accelerates the ionic movement.

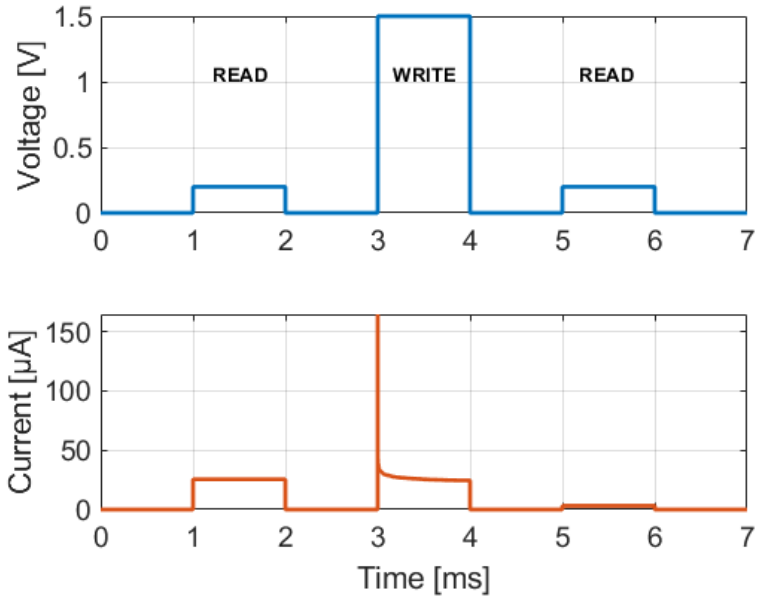

Fig. 3.6: Pulse Characteristics for RESET: Read at 0.2 V and write at 1.5 V

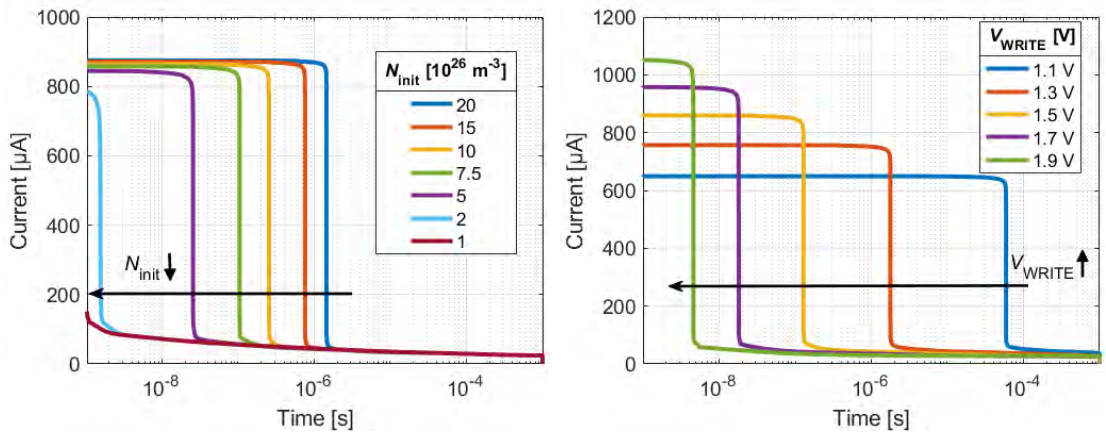

(a) **(b)**

Fig. 3.7: State and voltage dependency of the RESET delay time t_{RESET} a) at different initial HRS ($V_{\mathrm{WRITE}} = 1.5$ V and b) for one initial LRS state and different WRITE pulse voltages. Note that the different initial current in b) is only due to the different applied voltages.

Chapter 4

Variability

The JART VCM v1b Variability module includes device-to-device variability as well as cycle-to-cycle variability. Both variability's are based on the variation of the following parameters values:

- Minimum oxygen concentration in the disc $N_{\text{disc, min, var}}$
- Maximum oxygen concentration in the disc $N_{\text{disc, max, var}}$
- Radius of the filament r_{var}
- Length of the disc l_{var}

For the device-to-device variability, the cells are initialized statistically by varying the parameter values mentioned above. For the cycle-to-cycle variability, the same parameters are changed during the simulation, either directly or coupled with the switching processes.

In order to simulate the device-to-device and cycle-to-cycle variability, an additional parameter set file is required. An example for this file is shown in the Listing. 4.1. The table shows the values of the aforementioned parameters for two cells at discrete times (displayed in the first column (in seconds)). The parameter set file is not generated within the Verilog-A code of the compact model. Auxiliary software (Python, MATLAB) has to be used. The table including its linkage towards the device-to-device and cycle-to-cycle-variability will be discussed in the following. For further readings, please refer to [5].

```
pset1 paramset{}                                                                    1
time   Ndiscmin0  Ndiscmax0  rnew0    lnew0  Ndiscmin1  Ndiscmax1  rnew1    lnew1  ...  2
0      0.0076     20.5       44.3e-9  0.401  0.009      17.3       41.5e-9  0.451  ...  3
2.6    0.0070     19         46.1e-9  0.428  0.0094     17.9       40.9e-9  0.471  ...  4
5.2    0.0068     19.3       45.9e-9  0.42   0.0085     18.0       41.1e-9  0.448  ...  5
```

```
7.8    0.0071     20          44.9e-9  0.379  0.0087     16.4        42.1e-9  0.459  ...   6
...    ...        ...         ...      ...    ...        ...         ...      ...    ...   7
}                                                                                          8
```

Listing 4.1: Exemplary parameter set file for the device-to-device and cycle-to-cycle variability.

4.1 Device-to-Device Variability

The variation of the parameter set consisting of $N_{\text{disc, min, var}}$, $N_{\text{disc, max, var}}$, r_{var} l_{var} for each device can be best depicted by choosing their values from their respective Gaussian distributions. It is recommended to truncate the Gaussian distribution in order to keep the quantities within reasonable ranges. In Listing 4.1, the parameter values at (`time = 0`) depict the device-to-device variability for two devices (e.g. `Ndiscmin0` for the minimum disc oxygen vacancy concentration in cell0 or `Ndiscmin1` for the minimum disc oxygen vacancy concentration in cell1 etc.).

4.2 Cycle-to-Cycle Variability

The cycle-to-cycle variability is a bit more complicated. The change of the parameters during the SET and RESET for each cycle is depicted as a one dimensional random walk process. Here, the parameter value ξ_{k} given at the time step k is determined by

$$\xi_{\text{k}} = \xi_{\text{k-1}} \cdot (1 \pm \Delta\xi_{\text{max}} \cdot P). \tag{4.1}$$

$\xi_{\text{k-1}}$ denotes the parameter value of the previous time step. $\Delta\xi_{\text{max}}$ is the maximum possible change of $\xi_{\text{k-1}}$ and P is a random number between 0 and 1, which scales the change of the parameter. As for $N_{\text{disc, min, var}}$, $\Delta\xi_{\text{max}}$ is set to 90 %, while for the other quantities, $\Delta\xi_{\text{max}}$ is set to 10 %. While $N_{\text{disc, min}}$ and $N_{\text{disc, max}}$ are changed directly at the start of the SET and RESET regime, r_{var} and l_{var} are linked to the state variable N_{disc} and change gradually during the switching, until the maximum or minimum oxygen vacancy concentration is reached. In the SET direction, both quantities are calculated as

$$r_{\text{var}} = r_{\text{old}} + (r_{\text{new}} - r_{\text{old}}) \left(\frac{N_{\text{disc}} - N_{\text{disc, old}}}{N_{\text{disc, max, var}} - N_{\text{disc,old}}} \right) \tag{4.2}$$

and

$$l_{\text{var}} = l_{\text{old}} + (l_{\text{new}} - l_{\text{old}}) \left(\frac{N_{\text{disc}} - N_{\text{disc, old}}}{N_{\text{disc, max, var}} - N_{\text{disc,old}}} \right), \tag{4.3}$$

while the RESET direction, both quantities are calculated as

$$r_{\text{var}} = r_{\text{old}} + (r_{\text{new}} - r_{\text{old}}) \left(\frac{N_{\text{disc, old}} - N_{\text{disc}}}{N_{\text{disc, old}} - N_{\text{disc, min, var}}} \right) \tag{4.4}$$

and

$$l_{\text{var}} = l_{\text{old}} + (l_{\text{new}} - l_{\text{old}}) \left(\frac{N_{\text{disc, old}} - N_{\text{disc}}}{N_{\text{disc, old}} - N_{\text{disc, min, var}}} \right). \tag{4.5}$$

Here, r_{old} and l_{old} denote the values of r and l from the previous time step.
In Listing 4.1, starting from the second row (`time = 2.6`), the parameter values are generated according to Eq. 4.2 at each discrete time point. Particularly, the time points mark the beginning of the positive and negative voltage sweep. An example of the cycle-to-cycle variability is shown in Fig. 4.1, where a triangular voltage sweep between 1.3 V and -1.3 V with a sweep rate of 1 V/s is applied `cell0`. At the first zero crossing at 2.6 s in Fig. 4.1a, the parameter values formerly specified by the values at 0 s are updated to that specified at 2.6 s (c.f. 4.1). In the Verilog-A code, the different values of the parameters from the listing are updated each time at the zero voltage crossing.

```
@(cross(V(OE,AE) - 1.5e-5, +1))
begin
   rold=rvar;
   lold=lvar;
   Nold=Nreal;
end

@(cross(V(AE,OE) - 1.5e-5, +1))
begin
   rold=rvar;
   lold=lvar;
   Nold=Nreal;
end

if (V(AE,OE)<-2e-5) //SET at negative voltage
   begin
      rvar=rold+(rnew-rold)*((Nreal-Nold)/(Ndiscmax-Nold)); // Equation 19
      lvar=lold+(lnew-lold)*((Nreal-Nold)/(Ndiscmax-Nold)); // Equation 20
   end
else if (V(AE,OE)>2e-5) //RESET at positive voltage
```

```
   begin
      rvar=rold+(rnew-rold)*((Nold-Nreal)/(Nold-Ndiscmin)); // Equation 21
      lvar=lold+(lnew-lold)*((Nold-Nreal)/(Nold-Ndiscmin)); // Equation 22
   end
else
   begin
   end
}
```

In Fig. 4.2, a comparison of experimental and simulated device behavior is shown [5]. The simulations were performed using the parameters in Table 4.1. The first value of each entry represents the minimum value of this parameter, the second the mean value and the last represents the maximum value.

First row shows measured (a) and simulated (b) voltage sourced *I-V* sweeps. The second row shows the measured (c) and simulated (d) SET kinetics and the third row shows the measured (e) and simulated (f) RESET kinetics. The blue circles represent the experimental RESET kinetics starting from LRS between 1.85 kΩ and 2.22 kΩ (LRS range I (experimental)) while the green points represent the RESET kinetics starting from LRS between 1.52 kΩ and 1.67 kΩ (LRS range II (exp.)). The solid lines represent the RESET kinetics of the deterministic model using the parameters from Table I and the initial LRS as detailed in [4]. The blue box plots show the RESET kinetics for the variability model for an LRS range between 1.92 kΩ and 2.04 kΩ (LRS range I (simulated)) while the green box plots show the RESET kinetics of the variability model for an LRS range between 1.58 kΩ and 1.67 kΩ (LRS range II (sim.)). The fourth row ((g) and (h)) shows the measured and simulated endurance behavior over 1000 cycles. Generally, a good qualitative agreement between measurement and simulation is observed not only for device properties like LRS, HRS, SET and RESET voltages and switching kinetics but also for the statistical behavior of these properties. A more detailed explanation of the chosen parameters and the experimental procedure can be found in [5].

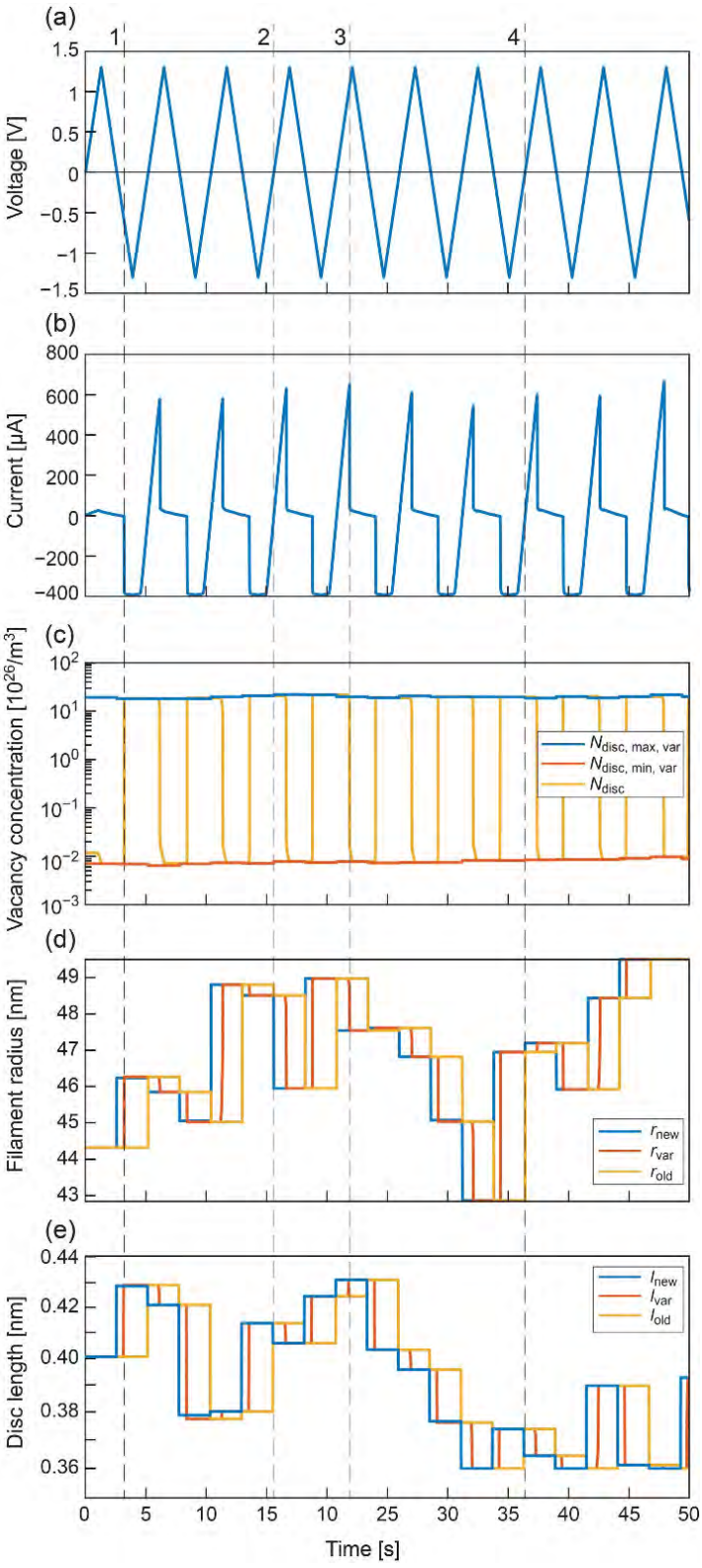

Fig. 4.1: The functionality of the cycle-to-cycle variability is shown during an $I-V$- sweep simulation with a current compliance of -400 μA. The graphs (a) to (e) show different properties of the simulations during the simulation with aligned time axes. (a) The applied voltage is swept between -1.3 V and +1.3 V with a sweep rate of 1 V/s. (b) shows the resulting current at the same time points. (c) shows the model parameters N_{disc}, $N_{\text{disc,max,var}}$ and $N_{\text{disc,min,var}}$;(d) shows r_{new},l_{var} and r_{old} and (e) shows the parameters l_{new}, l_{var} and l_{old}. Taken from [5]

	$N_{\text{min, var}}$ $\left[10^{23}\text{m}^{-3}\right]$	$N_{\text{max, var}}$ $\left[10^{26}\text{m}^{-3}\right]$	r_{var} [nm]	l_{var} [nm]
(b)	4 / 8 / 16	0.10 / 0.15 / 0.2	40.5 / 45 / 49.5	0.36 / 0.4 / 0.44
(d)	4 / 8 / 16	18 / 20 / 22	40.5 / 45 / 49.5	0.36 / 0.4 / 0.44
(f)	4 / 8 / 16	18 / 20 / 22	40.5 / 45 / 49.5	0.36 / 0.4 / 0.44
(h)	4 / 8 / 25	0.39 / 0.4 / 0.41	40.5 / 45 / 49.5	0.36 / 0.4 / 0.44

Table 4.1: Parameter Ranges for Figure 4.2

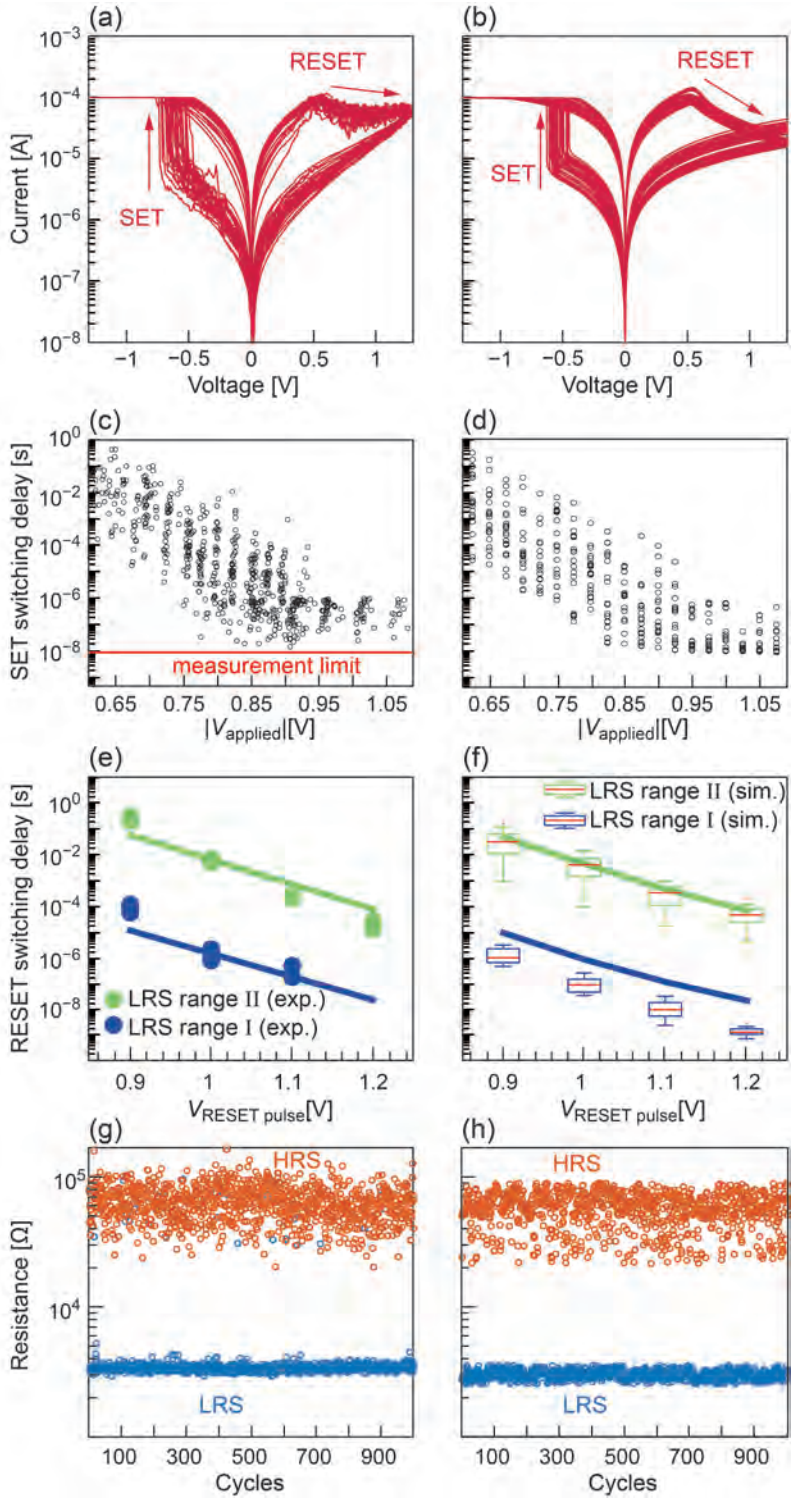

Fig. 4.2: Measured device characteristics alongside results obtained using the compact model extended with device-to-device and cycle-to-cycle variability.

Chapter 5

Random Telegraph Noise

The JART VCM v1b Variability Model has been extended with a RTN module, which accounts for the observable random fluctuation in conductivity of the VCM cell during a read. The noise is incorporated into the compact model by utilizing a state machine which describes the change of the oxygen vacancy numbers by single oxygen vacancy transitions. The state machine is illustrated in Fig. 5.1. At a given time, the initial state 0 has a probability of $p_2/2$ to either change into the state +1 (increase by one oxygen vacancy) or to the state -1 (decrease by one oxygen vacancy). State 0 also has a probability of 1-p_2 to remain unchanged. In state +1 (or -1), a change into the initial state 0 can happen with the probability p_1, or the state can remain unchanged with a probability of p_3, or the state changes into the +2 state (increase by one oxygen vacancy) with the probability 1-p_2-p_1. The probabilities are chosen such that, the state machine aims to relax into the initial state 0.

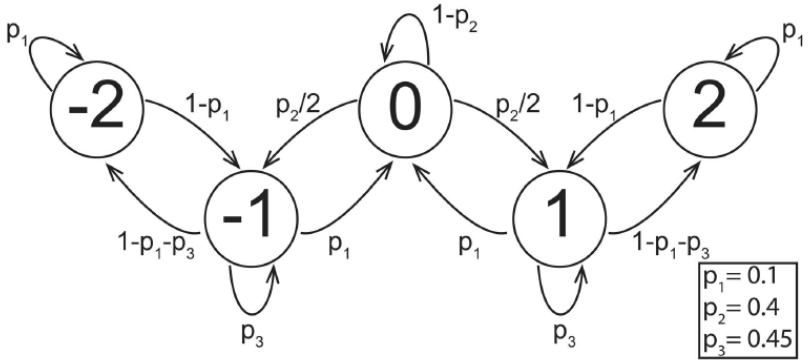

Fig. 5.1: State machine showcasing the different possible states around the initial number of oxygen vacancies in the disc (0) and the transition probabilities between those states. Taken from [6].

The states are limited between -2 and 2.

The values for p_1, p_2 and p_3 can be changed in the Verilog-A code. Furthermore, during the transient simulation, the state machine is evaluated at equidistant time points. These time points are determined by the frequency `freq`, which is generated from a normal distribution for each device.

```
//Creating Jump Distribution
p1 = 0.1;
p2 = 0.4;
p3 = 0.45;

//Random Frequency for the timer of the state machine
uniqueseed=$random;
freq=$rdist_normal(uniqueseed,50,50);
```

The following Verilog-A code shows the implementation of the state machine into Verilog-A. The `timer`-function specifies, that starting from $t = 0$, the state machine will be evaluated after every `1/freq`.

```
@(timer(0,1/freq)) // start, period (should fit to large jumps from experiments)
begin
     jump=0; // cell is randomly initialised with -2 -1 0 1 or 2
     randnum_jump = abs($random() % 1000); //0.0001-0.9999
     p_jump = randnum_jump/1000;
  if (jump_old == -2)
     begin
     numberminustwos=numberminustwos+1;
        if (p_jump < p1)
           jump = -2;
        else
           jump = -1;
     end
  else if (jump_old == -1)
     begin
     numberminusones=numberminusones+1;
        if (p_jump < p1)
           jump = -2;
        else if (p_jump < p3)
           jump = -1;
        else
           jump = 0;
      end
  else if (jump_old == 0)
```

```
    begin
    numberzeros=numberzeros+1;
       if (p_jump < p2)
             begin
             randnum_jump2 = abs($random() % 1000);
             p_jump_2 = randnum_jump2/1000;
             if (p_jump_2 > 0.5)
                jump = -1;
             else
                jump = 1;
          end
       else
          jump = 0;
    end
 else if (jump_old == 1)
    begin
    numberplusones=numberplusones+1;
       if (p_jump < p1)
          jump = 2;
       else if (p_jump < p3)
          jump = 1;
       else
          jump = 0;
    end
 else if (jump_old == 2)
    begin
    numberplustwos=numberplustwos+1;
       if (p_jump < p1)
          jump = 2;
       else
          jump = 1;
    end

 jump_old=jump;
 Nnoise_change = jump/(A*lnew*1e-9*1e26);
```

Simulated current traces of the HRS for three different devices are depicted in Fig. 5.2. Here, a voltage pulse of 0.35 V was applied to the devices for a duration of 2 s. Note that the conductivity of each device is different due to the device-to-device variability (see Section 4.1). The currents also exhibit different magnitudes of noise as well as a variation in the frequency. In the orange curve for instance, all possible states (-2, -1, 0, +1 and +2) can be seen.

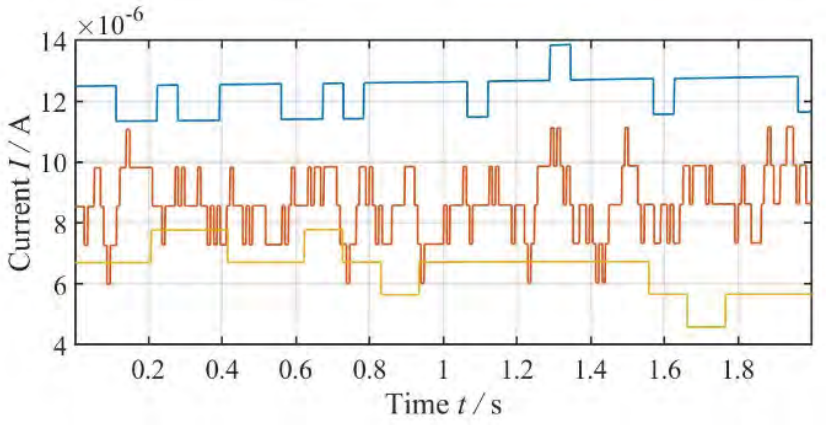

Fig. 5.2: Simulated current traces for three devices measured at 0.35 V. The signals all show the characteristic current jumps between distinct levels around a constant median current. Taken from [6].

Chapter 6

Exemplary Spectre Simulations

The aim of this chapter is to provide a number of exemplary Spectre decks for new users of the JART models. The first example we want to show is the simulation of a SET kinetic (see also Fig. 3.5 (b)). The Spectre deck for performing the simulation can be seen in the listing. It assumes that the Verilog-A model is in the same location as the Spectre file. The code applies a pulse with a rise time of 100 ns and a voltage amplitude of "V_{app}" until the end of the simulation. The variable V_{app} is then swept between -0.6 V and 1.1 V.

```
simulator lang=spectre
global 0
parameters Vapp=1

A0Vwl0 (A0wl0 0) vsource type=pwl delay=0 wave=[ 0 0 100n Vapp ]
A0reramw0b0it0 (A0wl0 0) JART_VCM_1b_det

swp sweep param=Vapp values=[-0.6 -0.7 -0.8 -0.9 -1.1]{
   tran tran stop=1 errpreset=conservative maxstep=1e-4
}
saveOptions options save=all currents=all saveahdlvars=all
ahdl_include "veriloga.va"
```

The resulting current traces can be seen in Fig. 6.1. As expected higher voltages lead to a much faster switching. A voltage difference of only 0.5 V leads to a 5 orders of magnitude difference in switching times.
In the second example, we will examine the effect of using a transistor in a 1T1R structure as a variable current compliance during SET. The transistors are modeled by a BSIM 4 model with the parameters of [14]. A schematic of the structure can be seen in Fig. 6.2 (b). The

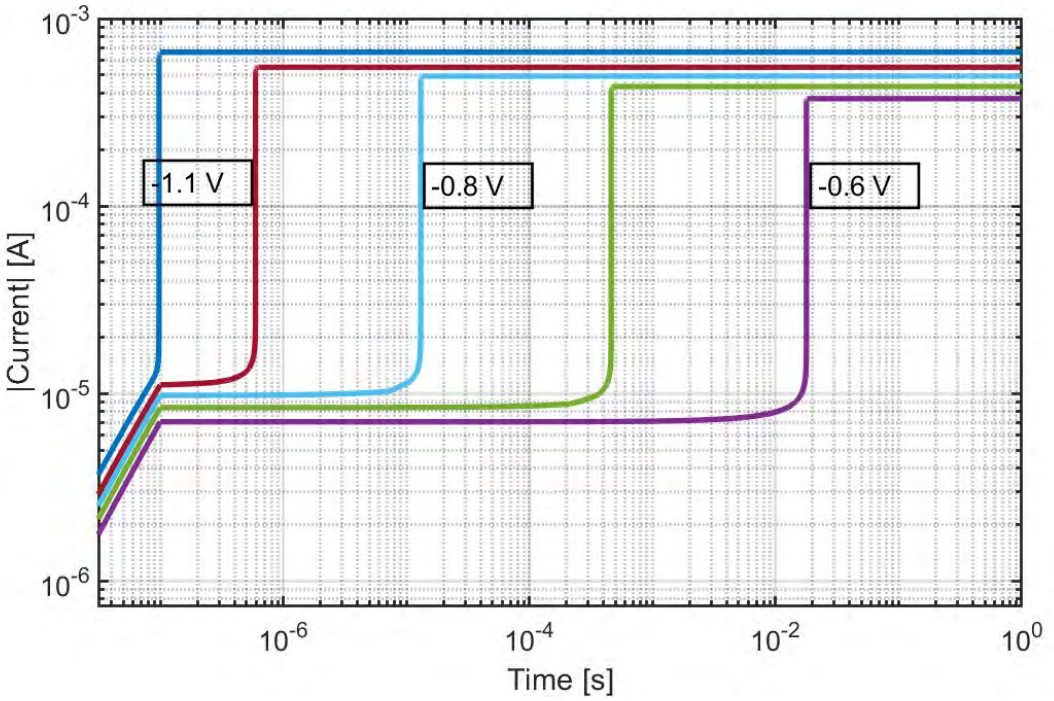

Fig. 6.1: Current over voltage plot showing the exponential dependence of the SET time on the applied voltage for voltages between -0.6 V and -1.1 V.

Spectre deck for performing the simulation can be seen in the below listing. It assumes that the Verilog-A model and the transistor model file are in the same location as the Spectre file. The resulting current traces can be seen in Fig. 6.2 (a). The simulation consists of a first readout of the 1T1R structure from 1 ns to 10 ns, which confirms an initial current of around 3 μA in all cases. Afterwards the a SET voltage of 1 V is applied to the ohmic electrode (OE) of the ReRAM cell and the gate voltage of the transistor is set to different values between 0.5 V and 1.3 V. After 1 μs the 1T1R structure is read out again revealing the different current levels, which correspond to different programmed resistances. The green curve corresponds to the current response for the highest gate voltage while the blue curve corresponds to the current response for the smallest gate voltage.

```
simulator lang=spectre
global 0
parameters VGATE=1 VSET=1

VGate (Gate 0) vsource type=pwl delay=0 wave=[ 0 0 1n 1 10n 1 11n VGATE 1u VGATE
    1.001u 1]
```

```
VOE (OE 0) vsource type=pwl delay=0 wave=[ 0 0 1n 0.3 10n 0.3 11n VSET 1u VSET
    1.001u 0.3 ]
ReRAM (AE OE) JART_VCM_1b_det
T (AE Gate 0 0) ptm_32nmHP_bulk_nmos w=32n l=32n

swp sweep param=VGATE values=[0.5 0.7 0.9 1.1 1.3]{
   tran tran stop=2u errpreset=conservative maxstep=1e-8
}

saveOptions options save=all currents=all saveahdlvars=all
ahdl_include "veriloga.va"
include "transistor_modelfile"
```

As expected higher gate voltages lead to a faster switching but also to a stronger SET as the current compliance of the transistor is set to higher maximum currents.

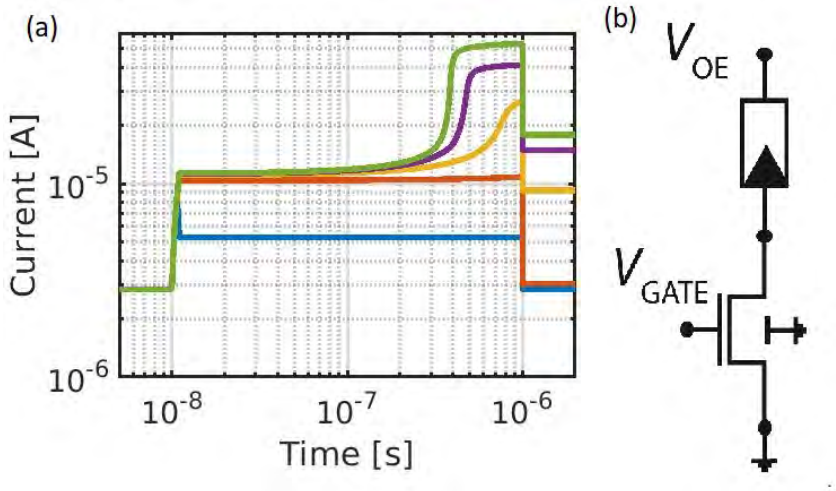

Fig. 6.2: (a) Current over time plot showing the programming of a ReRAM cell in a 1T1R structure using different SET voltages at a constant gate voltage. (b) shows the schematic of the 1T1R structure.

References

[1] A. Hardtdegen, C. L. Torre, F. Cuppers, S. Menzel, R. Waser, and S. Hoffmann-Eifert, "Improved Switching Stability and the Effect of an Internal Series Resistor in HfO_2/TiO_X Bilayer ReRAM Cells," *IEEE Transactions on Electron Devices*, vol. 65, pp. 3229–3236, Aug. 2018.

[2] C. La Torre, *Physics-Based Compact Modeling of Valence-Change-Based Resistive Switching Devices*. PhD thesis, RWTH Aachen University, 2019.

[3] K. Fleck, N. Aslam, S. Hoffmann-Eifert, V. Longo, F. Roozeboom, W. M. M. Kessels, U. Böttger, R. Waser, and S. Menzel, "The influence of non-stoichiometry on the switching kinetics of strontium-titanate ReRAM devices," *Journal of Applied Physics*, vol. 120, p. 244502, Dec. 2016.

[4] F. Cüppers, S. Menzel, C. Bengel, A. Hardtdegen, M. von Witzleben, U. Böttger, R. Waser, and S. Hoffmann-Eifert, "Exploiting the switching dynamics of HfO_2-based ReRAM devices for reliable analog memristive behavior," *APL Materials*, vol. 7, p. 091105, Sept. 2019.

[5] C. Bengel, A. Siemon, F. Cuppers, S. Hoffmann-Eifert, A. Hardtdegen, M. von Witzleben, L. Hellmich, R. Waser, and S. Menzel, "Variability-aware modeling of filamentary oxide-based bipolar resistive switching cells using SPICE level compact models," *IEEE Transactions on Circuits and Systems I: Regular Papers*, pp. 1–13, 2020.

[6] S. Wiefels, C. Bengel, N. Kopperberg, K. Zhang, R. Waser, and S. Menzel, "HRS instability in oxide-based bipolar resistive switching cells," *IEEE Transactions on Electron Devices*, vol. 67, pp. 4208–4215, Oct. 2020.

[7] R. Waser, R. Bruchhaus, and S. Menzel, "Redox-based Resistive Switching Memories," in *Nanoelectronics and Information Technology (3rd edition)* (R. Waser, ed.), pp. 683–710, Wiley-VCH, 2012.

[8] C. Baeumer and R. Dittmann, "Redox-based memristive metal-oxide devices," in *Metal Oxide-Based Thin Film Structures* (G. Korotcenkov, ed.), pp. 489–522, Elsevier, Amsterdam, 2018.

[9] S. M. Sze and K. K. Ng, "Metal-Semiconductor Contacts," in *Physics of Semiconductor Devices*, pp. 134–196, John Wiley & Sons, Inc., Apr. 2006.

[10] A. R. Genreith-Schriever and R. A. D. Souza, "Field-enhanced ion transport in solids: Reexamination with molecular dynamics simulations," *Physical Review B*, vol. 94, Dec. 2016.

[11] S. Menzel, M. Waters, A. Marchewka, U. Böttger, R. Dittmann, and R. Waser, "Origin of the ultra-nonlinear switching kinetics in oxide-based resistive switches," *Advanced Functional Materials*, vol. 21, pp. 4487–4492, Sept. 2011.

[12] J. P. Strachan, A. C. Torrezan, F. Miao, M. D. Pickett, J. J. Yang, W. Yi, G. Medeiros-Ribeiro, and R. S. Williams, "State dynamics and modeling of tantalum oxide memristors," *IEEE Transactions on Electron Devices*, vol. 60, pp. 2194–2202, July 2013.

[13] T. Diokh, E. Le-Roux, S. Jeannot, M. Gros-Jean, P. Candelier, J. F. Nodin, V. Jousseaume, L. Perniola, H. Grampeix, T. Cabout, E. Jalaguier, M. Guillermet, and B. D. Salvo, "Investigation of the impact of the oxide thickness and RESET conditions on disturb in HfO2RRAM integrated in a 65nm CMOS technology," in *2013 IEEE International Reliability Physics Symposium (IRPS)*, IEEE, Apr. 2013.

[14] P. T. M. (PTM), "45nm bsim4 model card for bulk cmos: V0.0, http://ptm.asu.edu/," tech. rep., 2006.